J. Fluid Mech. (2018), *vol.* 850, *pp.* 5–17. © Cambridge University Press 2018
doi:10.1017/jfm.2018.465

Toward vortex identification based on local pressure-minimum criterion in compressible and variable density flows

Jie Yao[1] **and Fazle Hussain**[1,†]

[1]Department of Mechanical Engineering, Texas Tech University, Lubbock, TX 79409, USA

(Received 11 February 2018; revised 24 May 2018; accepted 25 May 2018;
first published online 2 July 2018)

We propose a dynamical vortex definition (the 'λ_ρ definition') for flows dominated by density variation, such as compressible and multi-phase flows. Based on the search of the pressure minimum in a plane, λ_ρ defines a vortex to be a connected region with two negative eigenvalues of the tensor $\boldsymbol{S}^M + \boldsymbol{S}^\vartheta$. Here, $\boldsymbol{S}^M$ is the symmetric part of the tensor product of the momentum gradient tensor $\nabla(\rho\boldsymbol{u})$ and the velocity gradient tensor $\nabla\boldsymbol{u}$, with $\boldsymbol{S}^\vartheta$ denoting the symmetric part of momentum-dilatation gradient tensor $\nabla(\vartheta\rho\boldsymbol{u})$, and $\vartheta \equiv \nabla\cdot\boldsymbol{u}$, the dilatation rate scalar. The λ_ρ definition is examined and compared with the λ_2 definition using the analytical isentropic Euler vortex and several other flows obtained by direct numerical simulation (DNS) – e.g. liquid jet breakup in a gas, a compressible wake, a compressible turbulent channel and a hypersonic turbulent boundary layer. For low Mach number ($M \lesssim 5$) compressible flows, the λ_2 and λ_ρ structures are nearly identical, so that the λ_2 method is still valid for low M compressible flows. But, the λ_ρ definition is needed for studying vortex dynamics in highly compressible and strongly varying density flows.

Key words: compressible flows, multiphase and particle-laden flows, vortex flows

1. Introduction

Turbulent flows are often viewed as a tangle of vortices or composed of coherent structures, and much of turbulence physics is interpreted using the concepts of vortex dynamics (Tennekes & Lumley 1972; Hussain 1986). Hence, vortex identification and visualization are crucial, and have formed the focus of numerous turbulent flow studies. Different from vorticity ($\boldsymbol{\omega} = \nabla\times\boldsymbol{u}$), a well-accepted mathematical definition of a 'vortex' is still lacking. As suggested in Jeong & Hussain (1995) (hereinafter JH), a vortex should at least satisfy the following requirements: (i) a vortex core must be a compact region with net circulation; and (ii) the identified vortex core must be Galilean invariant. During the past few decades, numerous vortex identification criteria have been proposed for incompressible flows (Hunt, Wray & Moin 1988; Chong, Perry & Cantwell 1990; Zhou *et al.* 1999; Haller 2005, JH), and most of them essentially use flow kinematics via the velocity gradient tensor $\nabla\boldsymbol{u}$. Among them,

† Email address for correspondence: fazle.hussain@ttu.edu

https://doi.org/10.1017/jfm.2018.465 Published online by Cambridge University Press

the most popularly used ones are: (i) Q, defined as the regions in which the vorticity magnitude prevails over the strain-rate magnitude $(\|\boldsymbol{\Omega}\|^2 - \|\boldsymbol{S}\|^2)/2$ (equivalent to the second invariant of $\nabla \boldsymbol{u}$ for incompressible flows); (ii) Δ (and also λ_{ci}), associated with the complex eigenvalues of $\nabla \boldsymbol{u}$; and (iii) λ_2: two negative eigenvalues of $\boldsymbol{S}^2 + \boldsymbol{\Omega}^2$, where $\boldsymbol{S}$ and $\boldsymbol{\Omega}$ are the symmetric and anti-symmetric components of $\nabla \boldsymbol{u}$ defined as $\boldsymbol{S} = (\nabla \boldsymbol{u} + (\nabla \boldsymbol{u})^{\mathrm{T}})/2$ and $\boldsymbol{\Omega} = (\nabla \boldsymbol{u} - (\nabla \boldsymbol{u})^{\mathrm{T}})/2$, respectively. The inter-relationships and differences among these criteria have also been extensively studied (Dubief & Delcayre 2000; Chakraborty, Balachandar & Adrian 2005; Pierce, Moin & Sayadi 2013, JH). The Q, Δ, λ_{ci} and λ_2 criteria give identical structures for axisymmetric vortices, and result in similar structures for most flows, if thresholds are suitably selected.

Turbulent flows with variable density are very common – for example, multi-phase and hypersonic flows. Currently, vortices in these flows are identified still using kinematic methods, which are either direct or slightly modified forms of vortex definitions developed for incompressible flows. The extendibility of the above commonly used vortex identification methods to compressible flows is discussed by Kolář (2009). The closely related Δ and λ_{ci} criteria, which can exclude the effect of non-zero divergence, can and have been directly applied to compressible flows (Pirozzoli, Bernardini & Grasso 2008; Kolář 2009; Shadloo, Hadjadj & Hussain 2015); however, the Q-criterion suffers from some ambiguity as it can represent either the positive second invariant of $\nabla \boldsymbol{u}$ or the positive values of $(\|\boldsymbol{\Omega}\|^2 - \|\boldsymbol{S}\|^2)/2$. To overcome this issue, several modifications of the Q-criterion have been proposed. For example, Kolář (2009) redefined a Q criterion with the deviatoric part of $\boldsymbol{S}$, namely, $Q_D = (\|\boldsymbol{\Omega}\|^2 - \|\boldsymbol{S}_D\|^2)/2$ with $\boldsymbol{S}_D = \boldsymbol{S} - 1/3 \cdot \mathrm{tr}(\boldsymbol{S}) \cdot \boldsymbol{I}$, and $\boldsymbol{I}$ is the identity matrix. Although this Q_D method can be unambiguously applied to compressible flows, a clear kinematic interpretation in three-dimensional flow is lacking. Recently, Kolář & Šístek (2015) proposed a Q_M method based on kinematic corotational and compressibility arguments, namely, $Q_M = Q + \Pi_s/2$, where Π_s is the second invariant of $\boldsymbol{S}$. In strong shear regions, Q_M seemingly works better than other methods due to additional correction term $(\Pi_s/2)$; however, the direct relation between the original Q-criterion and pressure expressed through the Poisson equation (JH) is lost. In the λ_2 method, the direct use of $\boldsymbol{S}^2 + \boldsymbol{\Omega}^2$ as an approximation of the pressure Hessian requires discarding some terms related to non-zero density gradients and divergence (Cucitore, Quadrio & Baron 1999). For variable density and compressible flows, we need a new vortex definition (see also Günther & Theisel 2017), which is not purely kinematic and can account for spatial variation of density as well as dilatation effects. In the next section, we propose an extension of the standard λ_2 criterion for flows dominated by density variation.

2. Theory

Physically, vortices are considered as compact regions with high vorticity (hence also circulation) (Wu, Ma & Zhou 2007, JH). Therefore, vorticity magnitude $|\boldsymbol{\omega}|$ seems to be a reasonable criterion for vortex identification. However, this approach, though fairly successful in wall-free shear flows or vortex interactions, like reconnection, may not always be suitable (JH). For example, in a boundary layer, the vorticity magnitude of the mean shear is indeed very high due to the no-slip condition. An alternative approach for vortex identification is through a search of the local pressure minimum, which necessarily occurs in the core of compact vortices due to the swirling motion. This led JH to propose the λ_2 criterion, which has been

https://doi.org/10.1017/jfm.2018.465 Published online by Cambridge University Press

demonstrated to successfully identify vortices and their interactions in numerous studies and situations. Incidentally, many other vortex identification criteria also depend on this pressure-minimum requirement (Hunt *et al.* 1988; Dubief & Delcayre 2000).

Following the same idea of the λ_2 criterion, we develop here the λ_ρ definition using local pressure minimum as the starting point. The compressible Navier–Stokes (N–S) equation is

$$\frac{\partial \rho u_i}{\partial t} + (\rho u_i u_k)_{,k} = -P_{,i} + \tau_{ik,k}, \tag{2.1}$$

where ρ is the density, u_i is the velocity component in the ith direction, P is the pressure, $\tau_{ij} = \mu(u_{i,j} + u_{j,i} - 2/3\vartheta\delta_{ij})$ is the viscous stress tensor, μ the dynamical viscosity and $\vartheta \equiv u_{k,k}$ the dilatation rate.

Taking the gradient of equation (2.1), we obtain

$$\frac{\mathrm{D}(\rho u_i)_{,j}}{\mathrm{D}t} + (\rho u_i)_{,k} u_{k,j} + (\rho\vartheta u_i)_{,j} = -P_{,ij} + \tau_{ik,kj}, \tag{2.2}$$

where $\mathrm{D}/\mathrm{D}t$ is the material derivative.

The symmetric part of equation (2.2) gives the equation for the pressure Hessian

$$\frac{\mathrm{D}S^m_{ji}}{\mathrm{D}t} - S^\tau_{ij} + S^M_{ij} + S^\vartheta_{ij} = -P_{,ij}, \tag{2.3}$$

with

$$S^m_{ij} = [(\rho u_i)_{,j} + (\rho u_j)_{,i}]/2, \tag{2.4a}$$

$$S^\tau_{ij} = [\tau_{ik,kj} + \tau_{jk,ki}]/2, \tag{2.4b}$$

$$S^M_{ij} = [(\rho u_i)_{,k} u_{k,j} + (\rho u_j)_{,k} u_{k,i}]/2, \tag{2.4c}$$

$$S^\vartheta_{ij} = [(\rho\vartheta u_i)_{,j} + (\rho\vartheta u_j)_{,i}]/2. \tag{2.4d}$$

As discussed by JH for incompressible flows, an inconsistency between the existence of a pressure minimum and the existence of a vortex core arises: (i) unsteady straining can create a pressure minimum without involving a vortical motion, as in sink flow; and (ii) viscous effects can eliminate the pressure minimum in a flow with vortical motion. These two effects also occur in compressible flows. In addition, compared to incompressible flows, the dilatation part in the viscous strain term can also create a pressure minimum without a vortical motion being involved, as in axisymmetric compressive flows driven by radial pressure gradient. By neglecting these effects, we expect to obtain an improved identifier of a vortex through the pressure-minimum criterion. Based on equation (2.3), we only consider the contribution of $\boldsymbol{S}^M + \boldsymbol{S}^\vartheta$ to identify a local pressure minimum in a plane, which requires two positive eigenvalues of the pressure Hessian tensor $P_{,ij}$ (JH). Hence, λ_ρ defines a vortex as a connected region with two negative eigenvalues of $\boldsymbol{S}^M + \boldsymbol{S}^\vartheta$. Here, $\boldsymbol{S}^\vartheta$ mainly accounts for the non-zero dilatation effect. Note that $\boldsymbol{S}^M$ can be further expressed as

$$S^M_{ij} = \rho(S_{ik}S_{kj} + \Omega_{ik}\Omega_{kj}) + \frac{\rho_{,k}}{2}(u_i u_{k,j} + u_j u_{k,i}). \tag{2.5}$$

The first term yields a density weighted λ_2 (denoted as $\bar{\lambda}_2$ herein), and the second term mainly accounts for the non-zero density gradients. For incompressible, uniform density flows, the λ_ρ definition simplifies to the desired $\bar{\lambda}_2$. The examples below show that in some cases $\bar{\lambda}_2$ is a satisfactory approximation of λ_ρ, and applies well for moderate M compressible flows or multi-phase flows.

https://doi.org/10.1017/jfm.2018.465 Published online by Cambridge University Press

3. Applications of definitions

Next, we evaluate the λ_ρ definition by applying it to a variety of flows involving density variations and compare with the λ_2 and λ_{ci} definitions.

3.1. *Isentropic Euler vortex*

This vortex is one of the few exact solutions for the Euler equations (Shu 1998). The velocity and temperature of the vortex are specified such that the entropy $E_S = p/\rho^\gamma$ is constant everywhere. The vortex is centred at the coordinate origin; and its azimuthal velocity is

$$v_\theta(r) = \frac{\beta r}{2\pi} \mathrm{e}^{(1-r^2)/2}. \tag{3.1}$$

The temperature, density and pressure are

$$T = 1 - \frac{(\gamma-1)\beta^2}{8\gamma\pi^2} \mathrm{e}^{1-r^2}, \quad \rho = T^{1/(\gamma-1)}, \quad p = \rho T = \rho^\gamma, \tag{3.2a–c}$$

and γ is the specific heat ratio.

Note that although it has density variation, the vortex is still incompressible due to zero velocity divergence – the density of each fluid particle remains constant. Hence, it is a good example to illustrate the difference between our dynamical λ_ρ and other kinematic definitions. Since the flow is planar, the Q, Δ and λ_2 definitions are equivalent (JH). For the λ_2 definition,

$$\boldsymbol{S}^2 + \boldsymbol{\Omega}^2 = \begin{bmatrix} -\dfrac{v_\theta v_\theta'}{r} & 0 \\ 0 & -\dfrac{v_\theta v_\theta'}{r} \end{bmatrix}, \tag{3.3}$$

where $v_\theta' = \partial v_\theta/\partial r$. The λ_2 vortex is the region with $v_\theta v_\theta'/r > 0$, i.e. $\partial v_\theta^2/\partial r > 0$.

For λ_ρ definition,

$$\boldsymbol{S}^M + \boldsymbol{S}^\vartheta = \begin{bmatrix} -\dfrac{\rho v_\theta v_\theta'}{r} & 0 \\ 0 & -\dfrac{\rho v_\theta v_\theta'}{r} - \dfrac{\rho' v_\theta^2}{r} \end{bmatrix}, \tag{3.4}$$

with $\rho' = \partial\rho/\partial r$.

Compared with λ_2, an additional density gradient term is involved in λ_ρ. Again, if ρ is constant (i.e. $\rho' = 0$), $\boldsymbol{S}^M + \boldsymbol{S}^\vartheta$ becomes $\rho(\boldsymbol{S}^2 + \boldsymbol{\Omega}^2)$, and the λ_ρ and λ_2 criteria are the same except for the scaling by ρ. If $\rho' > 0$, the vortex is defined as the region with $\rho v_\theta v_\theta'/r > 0$. Since density is always positive, the boundary of the vortex core identified by λ_ρ definition is the same as λ_2. Note that, even though the boundaries of λ_ρ and λ_2 are identical for $\rho' > 0$, their intensities (i.e. magnitudes) are different; this difference is important because of the unavoidable practical use of non-zero thresholds. On the other hand, if $\rho' < 0$, the core of λ_ρ vortex – the region with $\rho v_\theta v_\theta'/r + \rho' v_\theta^2/r > 0$ – is smaller than the λ_2 vortex core.

https://doi.org/10.1017/jfm.2018.465 Published online by Cambridge University Press

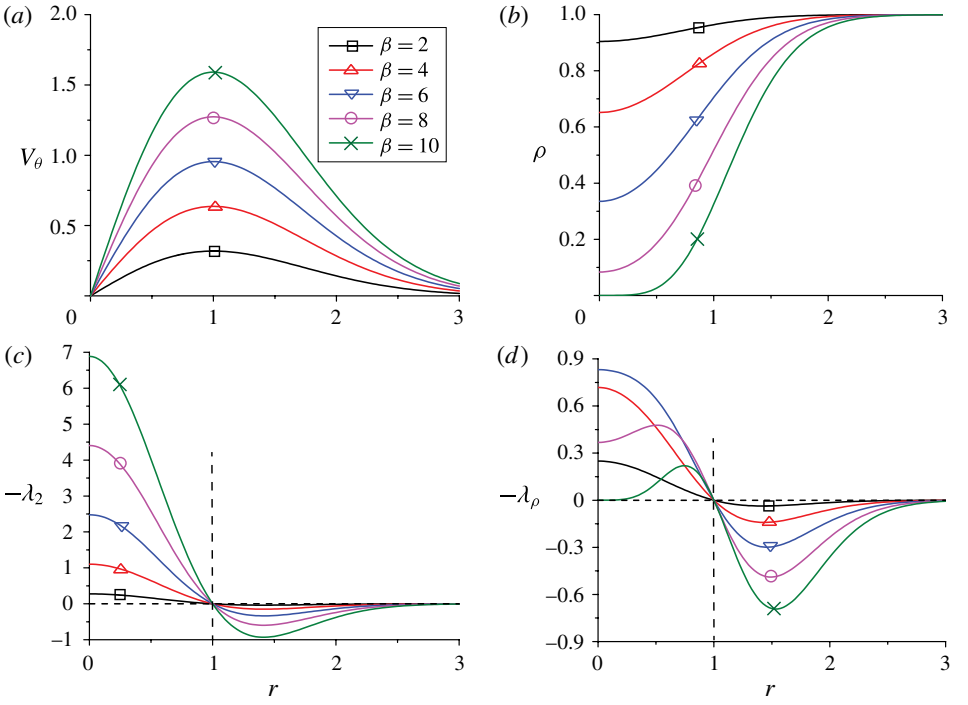


FIGURE 1. (Colour online) Isentropic Euler vortex: (*a*) azimuthal velocity; (*b*) density; (*c*) $-\lambda_2$ profiles; (*d*) $-\lambda_\rho$ profiles for different β values.

For this axisymmetric flow, the pressure is a function of radius r only. From the radial momentum equation, we get $P' = \partial P/\partial r = \rho v_\theta^2/r$. Hence, the pressure Hessian is

$$\begin{bmatrix} P'/r & 0 \\ 0 & \partial^2 P/\partial r^2 \end{bmatrix} = \begin{bmatrix} \dfrac{\rho v_\theta^2}{r^2} & 0 \\ 0 & \dfrac{2\rho v_\theta v_\theta'}{r} - \dfrac{\rho v_\theta^2}{r^2} + \dfrac{\rho' v_\theta^2}{r} \end{bmatrix}. \tag{3.5}$$

Clearly, compared with λ_2, the density gradient term in the λ_ρ criterion is necessary to better approximate the pressure Hessian. The main difference between λ_ρ and other vortex definitions is that λ_ρ is not a merely kinematic definition. The intensity of λ_ρ is determined not only by velocity, but also by density. In other words, kinematic vortex definitions, which are solely based on the velocity gradient $\nabla \boldsymbol{u}$, emphasize regions with strong swirling motions. But the λ_ρ definition, which also includes density variation effects, captures swirling motions with dynamical significance, i.e. having relatively strong momentum ($\rho \boldsymbol{u}$). This aspect may have importance in flow controls employing flow volume forcing as in plasma actuation (e.g. Shang *et al.* 2005).

Figures 1(*a*) and 1(*b*) display the azimuthal velocity and density profiles for the isentropic vortex with different β values. Figures 1(*c*) and 1(*d*) show the corresponding $-\lambda_2$ and $-\lambda_\rho$ profiles. Note that ρ' is positive for this flow, and the vortex core for both λ_2 and λ_ρ criteria is fixed for all β and is the region bounded by maximum azimuthal velocity ($r \leqslant 1$). The intensity of λ_2, which is

https://doi.org/10.1017/jfm.2018.465 Published online by Cambridge University Press

typically characterized by the magnitude of λ_2, increases monotonically with β, i.e. with increasing the angular velocity u_θ/r, For a low β case, the λ_ρ and λ_2 profiles are almost identical, because of small density variation. However, as β increases, the intensity of λ_ρ decreases, especially near the centre, due to decreased density and fluid momentum. Note that for $\beta \geqslant 10$, a nonzero threshold will denote a hollow vortex; in such cases, the hollow core should be discarded.

3.2. *Liquid jet breakup*

Consider a planar liquid jet breakup in a co-flowing gas at the time of ligament formation simulated in Zandian, Sirignano & Hussain (2018), where the gas-to-liquid density ratio $\hat{\rho} = 0.1$ and the gas-to-liquid viscosity ratio $\hat{\mu} = 0.0022$. Since the flow is incompressible in each phase, the λ_ρ definition is equivalent to the $\bar{\lambda}_2$ definition away from the interface. Typically, in order to clearly visualize vortical structures, a non-zero threshold is used to suppress noise and very weak or dynamically insignificant structures. Figures 2(*a*) and 2(*b*) show λ_2 and λ_ρ structures, respectively (to match the gas phase vortex structures between (*a*) and (*b*), the ratio of threshold of λ_ρ and λ_2 is set equal to the gas density). Generally, the vortex is much stronger in the gas phase as vorticity diffuses slower due to smaller gas viscosity. In the gas phase, the two definitions produce identical hairpin vortex structures. However, λ_ρ enhances the intensity of vortices in the liquid phase, due to its higher density. In figure 2(*b*), besides the strong hairpin vortices in the gas phase, the Kelvin–Helmholtz vortex in the liquid phase is captured by the λ_ρ method. Figure 2(*c*) shows the λ_ρ structure contours on the spanwise section (x–z plane) cutting through a ligament. Vortex dynamics associated with ligaments is central to understanding atomization (Zandian *et al.* 2018). Figures 2(*d*) and 2(*e*) compare λ_2 and λ_ρ structures near the ligaments. Since the momentum $\rho \boldsymbol{u}$ is conserved across the interface and gas-to-liquid density ratio $\hat{\rho} = 0.1$, the velocity in the liquid phase is approximately an order of magnitude smaller than in the gas phase. Hence, the vortex structures in the liquid phase based on λ_2 are much weaker than those in the gas phase and are barely visible. However, using the λ_ρ definition, the intensity of the λ_ρ structures in the ligament is enhanced. Hence, λ_ρ is more suitable for studying the dynamics of ligament and droplet formation.

3.3. *Compressible wake*

λ_ρ structures for a high-speed planar wake at free stream $M = 2$ (Hickey, Hussain & Wu 2016) is shown in figure 3(*a*). As we can see, λ_ρ captures both the roll and rib structures clearly. Figure 3(*b*) is the detailed comparison of the λ_2 and λ_ρ vortex structures in the boxed region in figure 3(*a*). Since the compressibility is weak (turbulent Mach number < 0.3), the λ_2 and λ_ρ structures almost coincide. Thus, the λ_2 criterion is still a good approximation of λ_ρ for low M compressible flows. To compare with other vortex identification methods, figure 3(*c*) further shows the structures identified with the λ_ρ and λ_{ci} criteria, the latter is calculated based on the traceless velocity gradient (Pirozzoli *et al.* 2008). As expected, for this low M flow, a very good congruence between λ_ρ and λ_{ci} is also observed.

3.4. *Compressible turbulent channel flows*

Direct numerical simulation (DNS) datasets of compressible turbulent channel flows with $M = 0.8$, 2 and 3 at bulk Reynolds number $Re_b = 3000$ are considered here.

https://doi.org/10.1017/jfm.2018.465 Published online by Cambridge University Press

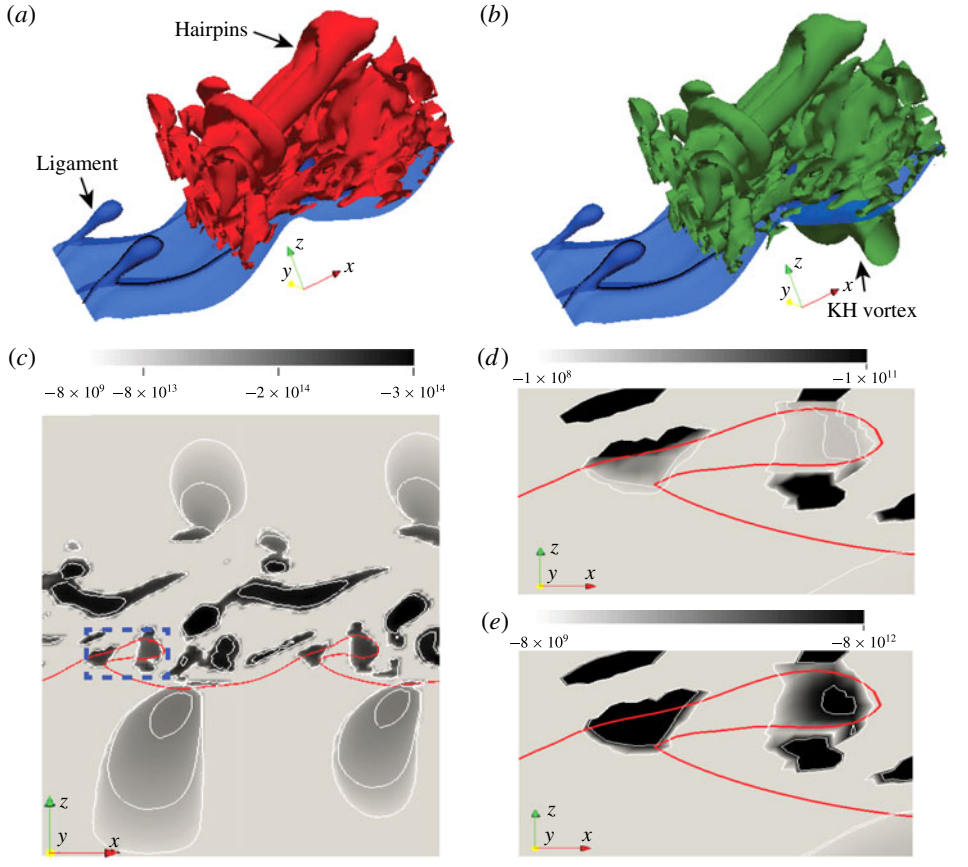


FIGURE 2. (Colour online) Liquid jet breakup: (*a*) λ_2 (red) and (*b*) λ_ρ (green) structures with blue denoting the liquid–gas interface; (*c*) λ_ρ contours on the spanwise cross-section; and detailed comparison between (*d*) λ_2 and (*e*) λ_ρ contours near the ligament (the boxed region in (*c*)).

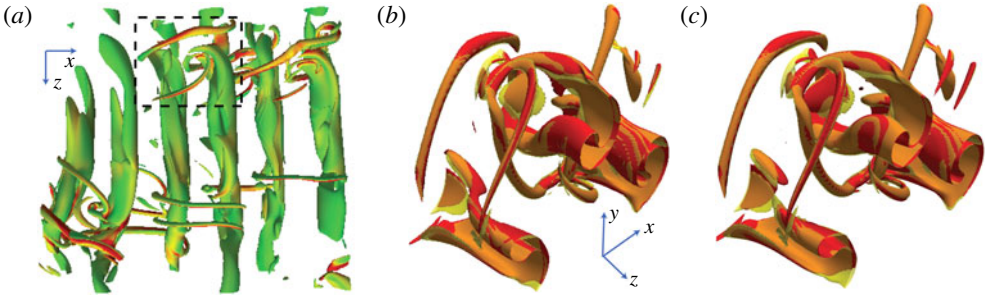


FIGURE 3. (Colour online) Compressible wake: (*a*) λ_ρ structures coloured by vorticity magnitude; detailed comparison between (*b*) λ_2 (red) and λ_ρ (brown) structures; (*c*) λ_{ci} (red) and λ_ρ (brown) structures in the boxed region marked in (*a*).

Figure 4 compares λ_ρ and λ_2 structures in the bottom half of the channel (the threshold is chosen as the root-mean-square (r.m.s.) value of each criterion at each M). Note that since the λ_{ci} agrees well with the λ_2 criterion for all these cases, here,

https://doi.org/10.1017/jfm.2018.465 Published online by Cambridge University Press

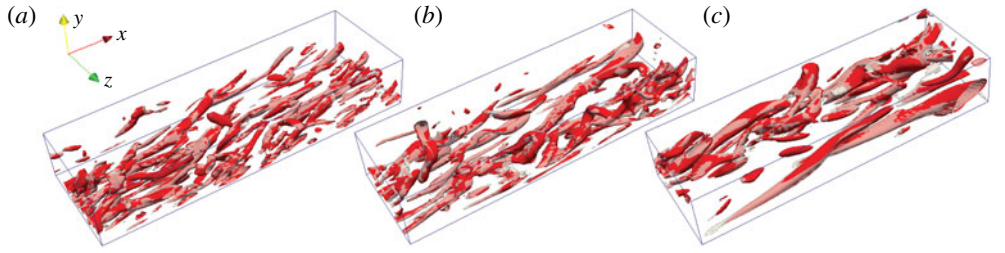


FIGURE 4. (Colour online) Compressible turbulent channel: comparison of λ_2 (red) and λ_ρ (grey) structures at (*a*) $M = 0.8$; (*b*) $M = 2$; and (*c*) $M = 3$.

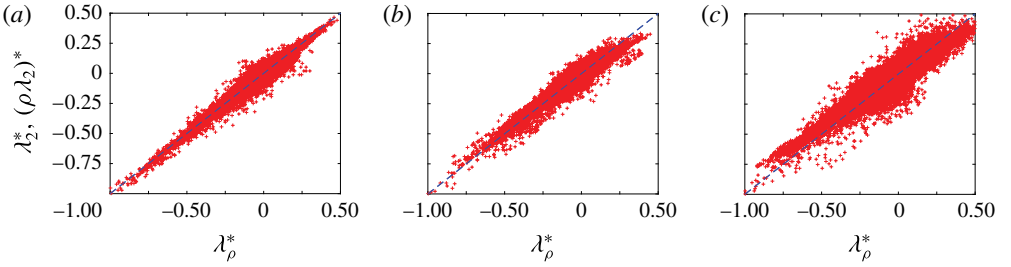


FIGURE 5. (Colour online) Scatter plots of normalized λ_ρ against λ_2 for compressible turbulent channel flows at (*a*) $M = 0.8$; (*b*) $M = 2$; and (*c*) $M = 3$. The quantities are normalized by their maximum values, and the dashed line denotes $\lambda_\rho/\max(|\lambda_\rho|) = \lambda_2/\max(|\lambda_2|)$.

only the λ_2 structures are compared. As M increases, the structures are more sparsely distributed and elongated, possibly due to higher shear at higher M. For M up to 3, the λ_2 and λ_ρ structures still coincide. The scatter plot of λ_ρ against λ_2 is shown in figure 5. As expected, the λ_ρ and λ_2 structures show a relatively strong correlation: for $M = 0.8$, if λ_ρ is high, so is λ_2; this correlation is reduced at $M = 3$, indicating that the λ_2 and λ_ρ structures would differ more for higher M flows.

3.5. *Hypersonic boundary layers*

As a final example, we consider the zero-pressure-gradient hypersonic turbulent boundary layer, which involves strong density variation in the wall-normal direction (for simulation details see Duan, Choudhari & Zhang (2016); Zhang, Duan & Choudhari (2016)). Figure 6(*a*) compares λ_2 and λ_ρ structures at $M = 6$ (the threshold is chosen as twice the r.m.s. value of each criterion). The λ_2 structures are located nearer to the wall, and are akin to the typical streamwise vortices observed in subsonic and supersonic boundary layers. As for λ_ρ, in addition to the near-wall structures, numerous coherent structures are captured far away from the wall. Figures 6(*b*) and 6(*c*) further compare structures of λ_ρ with $\bar{\lambda}_2$ and λ_{ci}, respectively. For this moderate $M(=6)$ hypersonic flow, the $\bar{\lambda}_2$ structures closely match the λ_ρ structures. The λ_{ci} structures, which seem to be quite similar to those of λ_2, differ from the λ_ρ structures mainly in the outer region of the boundary layer. These observations are further confirmed by the scatter plots. In figure 7(*a*), both the red (λ_ρ and λ_2) and yellow (λ_ρ and $\bar{\lambda}_2$) data points are mostly located along the 45° line; however, the

https://doi.org/10.1017/jfm.2018.465 Published online by Cambridge University Press

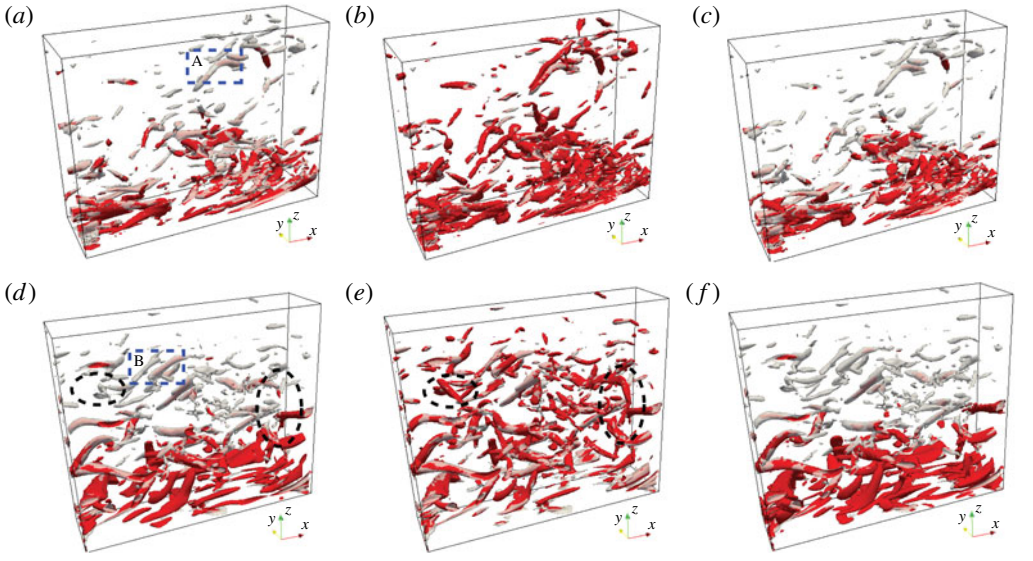


FIGURE 6. (Colour online) Hypersonic boundary layers: comparison of (*a*,*d*) λ_ρ (grey) and λ_2 (red) structures; (*b*,*e*) λ_ρ (grey) and $\bar{\lambda}_2$ (red) structures; (*c*,*f*) λ_ρ (grey) and $\bar{\lambda}_{ci}$ (red) structures for (*a–c*) $M = 6$ and (*d–f*) $M = 14$. Regions marked as A and B relate to later discussions of figure 8.

yellow data points are more compact, indicating closer similarity between λ_ρ and $\bar{\lambda}_2$ than between λ_ρ and λ_2. Surprisingly, for hypersonic flow at this $M = 6$, the λ_2 is still well correlated with $-\lambda_{ci}^2$ (figure 7*c*), indicating that the dilatation effect is not significant (note that, λ_{ci}^2 is employed here for dimensional consistency with λ_2). For $M = 14$, the difference between λ_2 and λ_ρ structures becomes even larger. Although $\bar{\lambda}_2$ is still a good approximation of λ_ρ, the disparity becomes more pronounced (see the circled region of figure 6*d*,*e*), showing the enhanced effects of density variation and dilatation at high M. The scatter plot in figure 7(*b*) also shows that even $\bar{\lambda}_2$ and λ_ρ are less correlated for this high M case. In addition, figure 7(*d*) shows that the difference between λ_{ci} and λ_ρ (as also between λ_{ci} and λ_2) becomes larger at this high M; this is clearly expected from the structure comparison shown in figure 6(*f*). Interestingly, λ_ρ (also λ_2) is almost around zero for the point where λ_{ci} is maximum. This discrepancy needs to be further investigated.

Generally, for hypersonic flows, λ_ρ captures more dynamical coherent structures than the other criteria, i.e. λ_2 and λ_{ci}. An interesting question arises as to whether these additional λ_ρ structures satisfy the basic requirement of vortices – namely, compact regions with high vorticity. To this end, figure 8 further shows the zoomed-in view of the λ_ρ structures in the outer boundary layer region along with vorticity lines for the $M = 6$ and 14 cases (marked as regions A and B in figure 6*a*,*d*). For each M, one λ_ρ structure (figure 8*a*,*c*) is a λ_2 structure also, and the other one (figure 8*a*,*c*) is only a λ_ρ structure. Note that all vorticity lines originate from the points, which are equally distributed on a circle centred at the $-\lambda_\rho$ peak in each structure marked as the + sign shown in the cross-sectional view, and then are extended in both directions away from this cross-section. The vorticity lines, generally along the λ_ρ structures, can also deviate from the vortical structures (as clearly shown in figure 8*b*). This observation that vorticity lines originating from the structure core do not necessarily

https://doi.org/10.1017/jfm.2018.465 Published online by Cambridge University Press

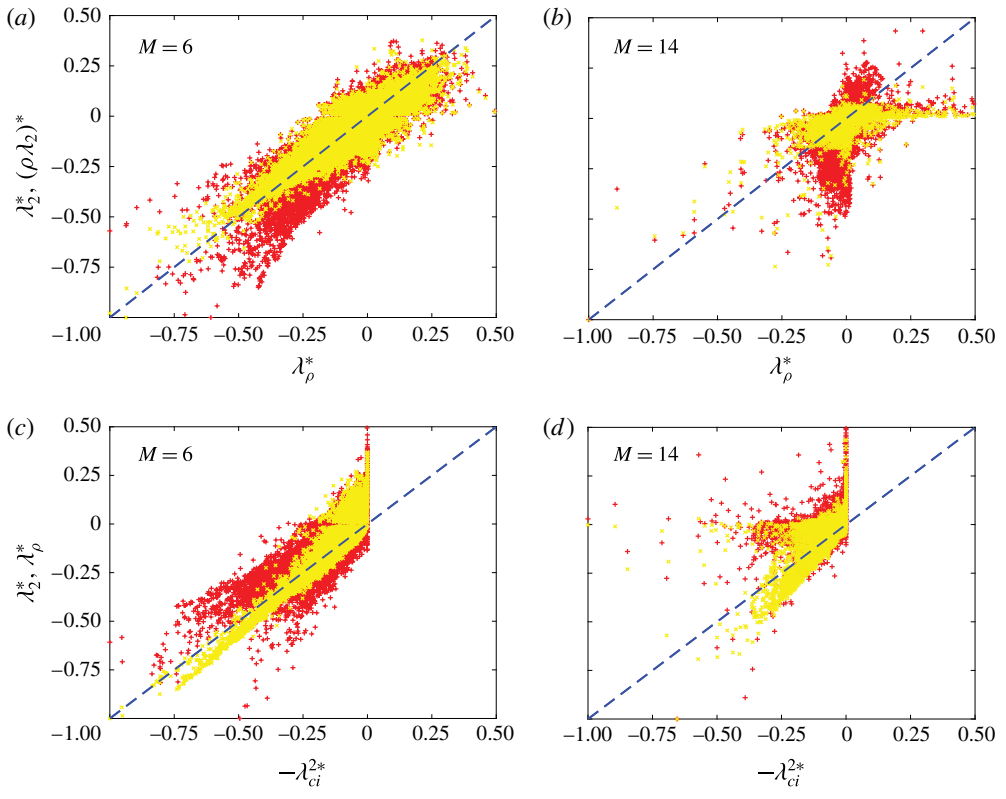


FIGURE 7. (Colour online) Scatter plots: (*a*,*b*) λ_ρ against λ_2 (red, +) and $\bar{\lambda}_2$ (yellow, *); and (*c*,*d*) $-\lambda_{ci}^2$ against λ_ρ (red) and λ_2 (yellow) for hypersonic turbulent boundary layers at (*a*,*c*) $M = 6$; (*b*,*d*) $M = 14$.

remain within the core but can cross the structure surface – contrary to popular belief – was also noted by Jeong *et al.* (1997) and Schoppa & Hussain (2002) in their studies of coherent structures in incompressible turbulent channel flows. Note that all λ_ρ structures, whether coinciding with λ_2 structures or not, are associated with relatively high vorticity concentrated on a collection of extended vortex lines. Therefore, the structures in the outer boundary layer region revealed by λ_ρ, although not necessarily by λ_2, are indeed vortices. How important these new-found structures are in the flow dynamics needs further study.

Recall that although vortices are associated with high vorticity, the reverse is not true; namely, high vorticity regions are not necessarily vortices (Dubief & Delcayre 2000; Günther & Theisel 2017, JH). For example, the laminar pipe flow has high vorticity near the wall but has no vortex. Hence, the λ_ρ and λ_2 (as well as Q, Δ and λ_{ci}, etc.) criteria are meant to identify vortices (with compact cross-sections), but not all regions of high vorticity, such as vorticity sheets or near-wall shear layers for wall-bounded flows. As an example, in figure 9 we further compare the iso-surfaces of: (*a*) vorticity magnitude $|\boldsymbol{\omega}|$; (*b*) λ_ρ; (*c*) $\lambda_\rho|\boldsymbol{\omega}|$, indicating correlation between λ_ρ and $|\boldsymbol{\omega}|$; and superimposed iso-surfaces of both λ_ρ and $\lambda_\rho|\boldsymbol{\omega}|$ from figures 9(*b*) and 9(*c*) excluding the near-wall region for the $M = 6$ hypersonic turbulent boundary layer; the same data as shown in figure 6. Note that the structure surfaces of $|\boldsymbol{\omega}|$, λ_ρ and $\lambda_\rho|\boldsymbol{\omega}|$ in figure 9 are plotted with the thresholds of 0.5, 1.0 and 2.0 times

https://doi.org/10.1017/jfm.2018.465 Published online by Cambridge University Press

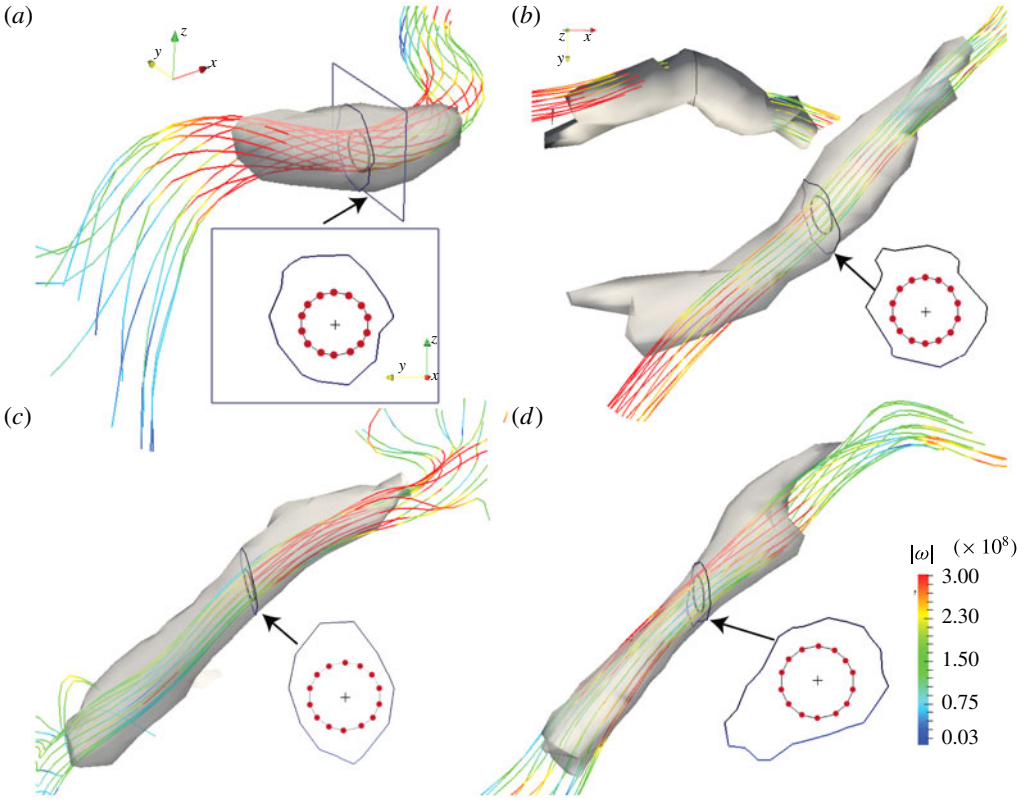


FIGURE 8. (Colour online) Zoomed-in view of the λ_ρ structures marked in the boxed regions (A,B) in figure 6 along with vorticity lines shaded by vorticity magnitude for (*a*,*b*) $M = 6$ and (*c*,*d*) $M = 14$. Note that the structures in (*a*,*c*) are λ_2 structures also, and (*b*,*d*) are λ_ρ structures only. The seeding points (red dots) for the vorticity lines are shown in the cross-sectional view with + indicating $-\lambda_\rho$ peak in each structure.

their own r.m.s. values in the domain, respectively; choices of these thresholds make the structures in the different figures of comparable sizes. Figure 9(*b*) shows that λ_ρ successfully identifies vortices with high vorticity in the outer region but excludes other regions of high vorticity like sheets in the near-wall region (included in figure 9*a*); that is, λ_ρ does not identify all regions of high vorticity but only vortices (which are associated with high vorticity and are compact). Clearly, therefore, high correlation between λ_ρ and $|\boldsymbol{\omega}|$ does not always represent vortices uniquely as it can also highlight regions with high vorticity but not vortices. This is why the structures near the wall in figure 9(*c*) are not identical to those in figure 9(*b*); but, indeed, there is good correlation between λ_ρ and $|\boldsymbol{\omega}|$ sufficiently away from the wall (figure 9*d*), where the background shear is relatively weak.

4. Conclusion

In summary, we present a new dynamical vortex definition for flows with a variable density effect, such as compressible and multi-phase flows. This new λ_ρ criterion, which is derived directly from the compressible momentum (N–S) equation, identifies the coherent local pressure minimum in a plane. Employing the analytically derived

https://doi.org/10.1017/jfm.2018.465 Published online by Cambridge University Press

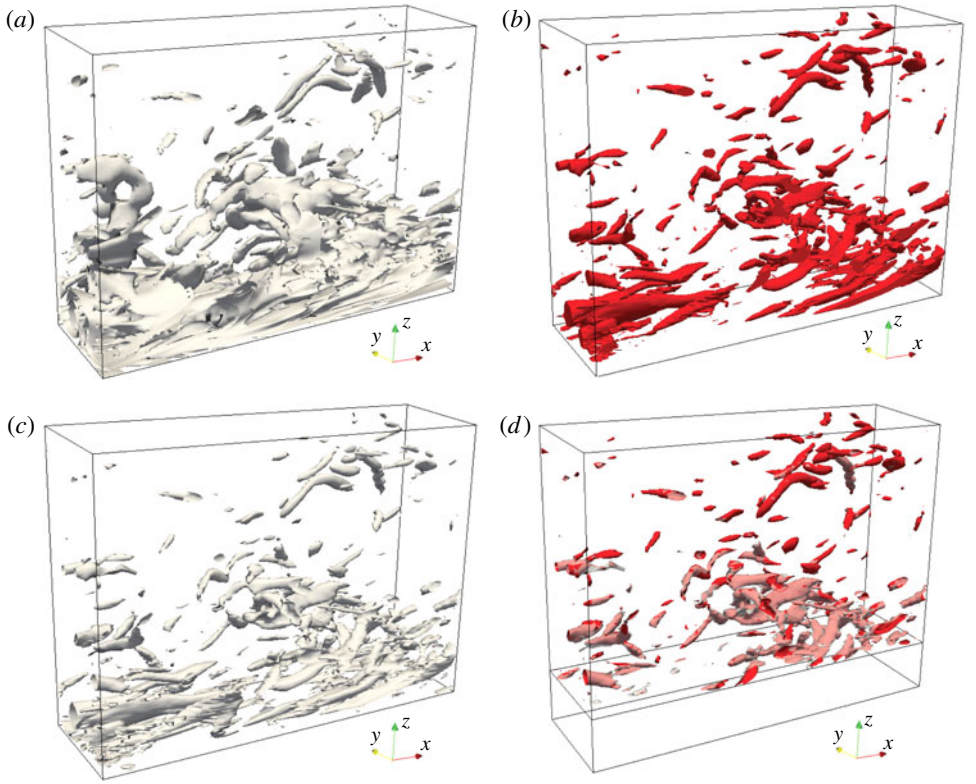


FIGURE 9. (Colour online) Iso-surfaces of (*a*) vorticity magnitude $|\boldsymbol{\omega}|$; (*b*) λ_ρ; (*c*) $\lambda_\rho|\boldsymbol{\omega}|$; and (*d*) superimposition of (*b*) and (*c*) in the outer region for the $M = 6$ hypersonic turbulent boundary layer shown in figure 6.

characteristics of the axisymmetric isentropic Euler vortex, we demonstrate that λ_ρ can better characterize the pressure Hessian than the kinematic criteria for variable density flows. λ_ρ is also examined and compared with the λ_2 and λ_{ci} for a variety of DNS data. As for the low M (i.e. <5) flows, where the compressibility effect is weak, very good congruence between λ_ρ and λ_2 (also λ_{ci}) are observed. For multi-phase and moderate hypersonic flows, $\bar{\lambda}_2$ works better than λ_2. However, the λ_ρ definition seems to be highly appropriate for studying vortex dynamics and flow control in highly compressible and strongly varying density flows and will be investigated in the future. In addition, it would be interesting to explore the applicability of the new λ_ρ definition for other complicated flows, such as turbulent reacting and supercritical flows (Chakraborty *et al.* 2017; Kim, Hickey & Scalo 2017). Systematic comparisons with other criteria, such as the average corotation method and Q_M (Kolář & Šístek 2015) are also needed.

Acknowledgements

We are grateful to A. Zandian, W. A. Sirignano, J.-P. Hickey, C. Zhang and L. Duan for providing us their DNS datasets and post-processing codes. We also thank E. Stout and X. Chen for helpful discussions.

https://doi.org/10.1017/jfm.2018.465 Published online by Cambridge University Press

REFERENCES

CHAKRABORTY, P., BALACHANDAR, S. & ADRIAN, R. J. 2005 On the relationships between local vortex identification schemes. *J. Fluid Mech.* **535**, 189–214.

CHAKRABORTY, N., WANG, L., KONSTANTINOU, I. & KLEIN, M. 2017 Vorticity statistics based on velocity and density-weighted velocity in premixed reactive turbulence. *J. Turbul.* **18** (9), 1–29.

CHONG, M. S., PERRY, A. E. & CANTWELL, B. J. 1990 A general classification of three-dimensional flow fields. *Phys. Fluids* A **2** (5), 765–777.

CUCITORE, R., QUADRIO, M. & BARON, A. 1999 On the effectiveness and limitations of local criteria for the identification of a vortex. *Eur. J. Mech. (*B*/Fluids)* **18** (2), 261–282.

DUAN, L., CHOUDHARI, M. M. & ZHANG, C. 2016 Pressure fluctuations induced by a hypersonic turbulent boundary layer. *J. Fluid Mech.* **804**, 578–607.

DUBIEF, Y. & DELCAYRE, F. 2000 On coherent-vortex identification in turbulence. *J. Turbul.* **1** (1), 011.

GÜNTHER, T. & THEISEL, H. 2017 The state of the art in vortex extraction. In *Computer Graphics Forum*. Wiley Online Library.

HALLER, G. 2005 An objective definition of a vortex. *J. Fluid Mech.* **525**, 1–26.

HICKEY, J.-P., HUSSAIN, F. & WU, X. 2016 Compressibility effects on the structural evolution of transitional high-speed planar wakes. *J. Fluid Mech.* **796**, 5–39.

HUNT, J. C., WRAY, A. A. & MOIN, P. 1988 Eddies, streams, and convergence zones in turbulent flows. *Center for Turbulence Research Report CTR-S88* 193.

HUSSAIN, A. K. M. F. 1986 Coherent structures and turbulence. *J. Fluid Mech.* **173**, 303–356.

JEONG, J. & HUSSAIN, F. 1995 On the identification of a vortex. *J. Fluid Mech.* **285**, 69–94.

JEONG, J., HUSSAIN, F., SCHOPPA, W. & KIM, J. 1997 Coherent structures near the wall in a turbulent channel flow. *J. Fluid Mech.* **332**, 185–214.

KIM, K., HICKEY, J.-P. & SCALO, C. 2017 Pseudophase-change effects in turbulent channel flow under transcritical temperature conditions. arXiv:1712.05777.

KOLÁŘ, V. 2009 Compressibility effect in vortex identification. *AIAA J.* **47** (2), 473–475.

KOLÁŘ, V. & ŠÍSTEK, J. 2015 Corotational and compressibility aspects leading to a modification of the vortex-identification q-criterion. *AIAA J.* **53** (8), 2406–2410.

PIERCE, B., MOIN, P. & SAYADI, T. 2013 Application of vortex identification schemes to direct numerical simulation data of a transitional boundary layer. *Phys. Fluids* **25** (1), 015102.

PIROZZOLI, S., BERNARDINI, M. & GRASSO, F. 2008 Characterization of coherent vortical structures in a supersonic turbulent boundary layer. *J. Fluid Mech.* **613**, 205–231.

SCHOPPA, W. & HUSSAIN, F. 2002 Coherent structure generation in near-wall turbulence. *J. Fluid Mech.* **453**, 57–108.

SHADLOO, M. S., HADJADJ, A. & HUSSAIN, F. 2015 Statistical behavior of supersonic turbulent boundary layers with heat transfer at $m = 2$. *Intl J. Heat Fluid Flow* **53**, 113–134.

SHANG, J. S., SURZHIKOV, S. T., KIMMEL, R., GAITONDE, D., MENART, J. & HAYES, J. 2005 Mechanisms of plasma actuators for hypersonic flow control. *Prog. Aerosp. Sci.* **41** (8), 642–668.

SHU, C.-W. 1998 Essentially non-oscillatory and weighted essentially non-oscillatory schemes for hyperbolic conservation laws. In *Advanced Numerical Approximation of Nonlinear Hyperbolic Equations*, pp. 325–432. Springer.

TENNEKES, H. & LUMLEY, J. L. 1972 *A First Course in Turbulence*. MIT Press.

WU, J.-Z., MA, H.-Y. & ZHOU, M.-D. 2007 *Vorticity and Vortex Dynamics*. Springer Science & Business Media.

ZANDIAN, A., SIRIGNANO, W. A. & HUSSAIN, F. 2018 Understanding liquid-jet atomization cascades via vortex dynamics. *J. Fluid Mech.* **843**, 293–354.

ZHANG, C., DUAN, L. & CHOUDHARI, M. 2016 Acoustic radiation from a mach 14 turbulent boundary layer. In *54th AIAA Aerospace Sciences Meeting*, pp. 2016–0048. AIAA.

ZHOU, J., ADRIAN, R. J., BALACHANDAR, S. & KENDALL, T. M. 1999 Mechanisms for generating coherent packets of hairpin vortices in channel flow. *J. Fluid Mech.* **387**, 353–396.

https://doi.org/10.1017/jfm.2018.465 Published online by Cambridge University Press